Creating charged domain walls in $PbTiO_3/LaCoO_{2.5}$ superlattices by oxygen vacancy engineering

Zhong Fang,[1,2] Yu-Jia Wang,[1,*] Xiang-Wei Guo,[1] Yun-Long Tang,[1] Yin-Lian Zhu,[3] and Xiu-Liang Ma[3,4]

[1]*Shenyang National Laboratory for Materials Science, Institute of Metal Research, Chinese Academy of Sciences, Wenhua Road 72, Shenyang 110016, China*

[2]*School of Materials Science and Engineering, University of Science and Technology of China, Wenhua Road 72, Shenyang 110016, China*

[3]*Songshan Lake Materials Laboratory, Dongguan 523808, Guangdong, China*

[4]*Institute of Physics, Chinese Academy of Sciences, Beijing 100190, China*

(Received 7 November 2023; accepted 18 December 2023; published 8 January 2024)

Charged domain walls in ferroelectric materials exhibit nontrivial electronic and transport properties, which have promising application in many electronic devices, such as high-density nonvolatile memories. Taking advantage of oxygen vacancy engineering, charged domain walls are introduced into the $PbTiO_3/LaCoO_{2.5}$ superlattice system, and the quasi-two-dimensional electron gas is formed near the domain walls, featuring an intrinsic *n*-type conductive characteristic. The charged domain walls can be erased by eliminating oxygen vacancies in the $LaCoO_{2.5}$, resulting in an insulating state. The proposed scheme of writing and erasing of charged domain walls may facilitate the development of domain wall based devices.

DOI: 10.1103/PhysRevB.109.035304

I. INTRODUCTION

Domain walls (DWs) in ferroelectric oxides, separating domains with different polarization orientations, possess nontrivial properties and different functionalities with respect to the surrounding domains due to the dimensionality reduction [1–3]. DWs are ubiquitous and can decisively affect physical phenomena such as polarization switching [4], electromechanical response [5,6], conductivity [7–9] and optical properties [10]. They can be created, shifted, and erased under external electric [3,11,12] or stress fields [13,14], which opens a promising paradigm for miniaturization of electronic devices, such as DW memories [15,16], switches [17], and diodes [18].

The relative orientation of the polarization across the individual DW determines the localized charge state. As a result, there are two types of DWs: the neutral domain walls (NDWs) and the charged domain walls (CDWs) [1]. NDWs usually possess lower formation energies and have been well studied for several decades [19–25]. CDWs are often in an energetically metastable state, with complex charge transport behaviors, which has triggered extensive exploration [26–30]. The versatile physical phenomena at the CDWs arise from the localized polarization discontinuity, which is responsible for the bound charges in the region with the formation of the depolarizing field. Such CDWs would be extremely unstable without a mechanism to screen the bound charges [26,31,32]. The most common screening mechanism is that free carriers such as electrons or holes compensate polarization charges at the CDWs, which mostly originates from electron transfer across the forbidden band gap or injection of external charges, leading to the formation of degenerate quasi-two-dimensional electron gas (q2DEG) or hole gas (q2DHG) [6,26,33,34]. The high-density degenerate gas formed at the CDWs dramatically enhances the conductivity and triggers the insulator-metal transition [34,35]. In addition, electronic band bending occurs at CDWs due to the imperfect compensation of bound charges by free carriers [6]. The bottom of the conduction band at the head-to-head CDWs should approach the Fermi level, so that the negative free electrons could accumulate to compensate for the positive bound charge. Analogously, at the tail-to-tail CDWs, the Fermi level should cross the top of the valance band, resulting in the accumulation of positive holes [26,27,33]. The lattice point defects, such as doping elements, cation vacancies, oxygen vacancies, etc., can also act to stabilize CDWs [8,36,37].

CDWs feature a variety of properties and wide potential for applications, and multiple strategies have been imposed on the engineering of CDW patterns [14,38,39]. Previous studies suggested CDWs can be introduced into the $BaTiO_3$ films by applying a repeated electric field with certain deviation from the intrinsic polarization direction [38]. CDWs can also be induced in films by applying appropriate strain gradients through mechanical loading [14]. Interfacial charge discontinuities in the ferroelectrics are prone to form electron (hole) gas, and different types of CDWs can be created in the $BiFeO_3$ layer of the $BiFeO_3/SrTiO_3$ superlattice by rationally designing the symmetric interfaces to avoid the formation of built-in electric field [34]. Recently, controlled electric field driven writing and migration of CDWs has been experimentally achieved by precise deposition of trilayer films with symmetric interfaces [3]. The introduction of oxygen vacancies in ferroelectrics has also been proved to be an effective means of creating CDWs. As early as 1998, Park and Chadi performed theoretical calculations to study the effect of different oxygen vacancies in the $PbTiO_3$ films on the polarization distribution and succeeded in introducing tail-to-tail CDWs [40]. The oxygen vacancies in $BaTiO_3$ could attract each other and accumulate, which ultimately induces the formation of

*Corresponding author: yjwang@imr.ac.cn

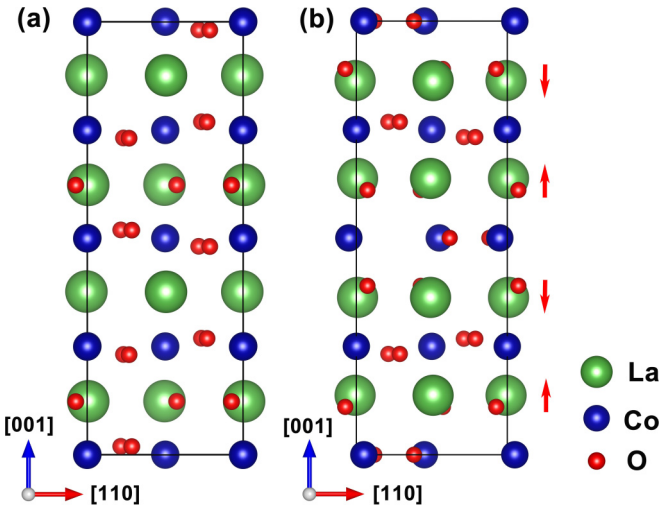

FIG. 1. Schematic structure of lanthanum cobaltate in the pseudocubic coordinates system. (a) $LaCoO_3$. (b) $LaCoO_{2.5}$. The red arrows represent the local ionic displacements.

tail-to-tail CDWs [39]. Experimentally, Geng *et al.* successfully obtained 71° and 109° tail-to-tail CDWs by introducing oxygen vacancy plates of different lengths into $BiFeO_3$ films [41]. Tian *et al.* further elucidated the impact of the size of the oxygen vacancy plates in this system on the CDWs structure through phase field simulations [42].

In fact, the method of introducing CDWs through oxygen vacancies in the ferroelectric film can only introduce tail-to-tail CDWs, which is inherently determined by the charge nature of the oxygen vacancies. In this work we utilized the oxygen vacancy layers in lanthanum cobaltate films to create head-to-head CDWs in $PbTiO_3$ films through rational interface design. The lanthanum cobaltate system has received widespread attention owing to its bias towards the formation of oxygen vacancy defects [43–50]. The bulk space group of the stoichiometric $LaCoO_3$ is $R\bar{3}c$, where the localized and total polarization along the z axis is 0 in the pseudocubic coordinate system, whereas nonstoichiometric films such as $LaCoO_{2.5}$ induce robust localized polarization along the z direction due to the existence of oxygen vacancy ordering, as shown in Fig. 1. Indeed, the stable existence of $LaCoO_{2.5}$ has been experimentally achieved in $PbTiO_3/LaCoO_{2.5}$ heterojunctions, and both experimental and theoretical calculations have shown that the oxygen vacancy ordering of $LaCoO_{2.5}$ in the heterojunction tends towards a parallel interface distribution [43]. The above experimental results provide strong support for the design of our superlattice model.

We propose a strategy of engineering oxygen vacancies to write and erase CDWs in a $PbTiO_3/LaCoO_{2.5}$ superlattice with symmetric interfaces. We successfully induced head-to-head CDWs into the $PbTiO_3$ layers, and the CDWs featured pronounced n-type conductivity characteristics, forming a q2DEG. The charge analysis revealed that the free electrons originated from the electron transport from the $LaCoO_{2.5}$ layers to the $PbTiO_3$ layers at the heterointerfaces. The introduction of the CDW in the $PbTiO_3$ layers is the result of the localized polarization of the LaO atomic layers at the interface, which is caused by the oxygen vacancies. After eliminating the oxygen vacancies in $LaCoO_{2.5}$ block, the CDWs in the $PbTiO_3$ layers are erased and the system is restored to the insulating state. Our results may provide an important theoretical basis for experimentally engineering the behavior of oxygen vacancies by different oxygen partial pressure annealing environments to achieve the writing and erasing of CDWs in ferroelectric superlattice and the metal-insulator transition.

The rest of the paper is organized as follows: In Sec. II, we describe the calculation method. In Sec. III, we further describe the calculation results of various models, perform detailed electronic structure analysis, and proposed an experimental scheme based on the calculation results. In Sec. IV, we provide a brief summary of the entire work.

II. CALCULATION METHOD

We have carried out the first-principles calculations in the framework of density of functional theory as implemented in the Vienna *ab initio* simulation package (VASP) [51,52]. The Perdew-Burke-Ernzerhof functional revised for solids (PBEsol) is the version of the generalized gradient approximation used as the exchange-correlation function for all calculations, as PBEsol provides a more accurate structure than its parent functional [53]. The plane wave cutoff energy was set to be 500 eV. Brillouin-zone integrations were performed with $4 \times 4 \times 1$ and $9 \times 9 \times 1$ Monkhorst-Pack k-point meshes for structural optimization and electronic structural calculations, respectively. The convergence conditions for the electronic self-consistent loop and the ionic relaxation loop were respectively set to be 10^{-5} eV and 0.01 eV Å^{-1}. The electronic-electronic correlations for Co ions are included by the Hubbard parameter with $U = 3.8$ eV [43,45]. According to the previous studies [46,54,55], the antiferromagnetic orders of $LaCoO_{2.5}$ were set as the G type: all the nearest-neighbor Co ions with antiparallel spins, while the $LaCoO_3$ of the epitaxial tensile strain state were set to ferromagnetic. According to our previous experimental results, the $PbTiO_3/LaCoO_{2.5}$ system was grown on the $SrTiO_3$ substrate [43]. Thus, we fixed the in-plane lattice parameters of the superlattices to be the same as the substrate.

III. RESULTS AND DISSCUSSION

In this work, we have constructed superlattice structures with different symmetric interfaces using $LaCoO_{2.5}$ and $PbTiO_3$. The paraelectric $PbTiO_3$ is adopted to construct the symmetric initial models. In fact, with respect to the composition of the interface and the arrangement of the oxygen vacancies, there are altogether four types of superlattice structures with symmetrical interfaces, as shown in Fig. 2. The interfaces of models (a) and (b) are both CoO_x/PbO, with the difference in the position of the oxygen vacancies. Analogously, the interfaces of models (c) and (d) are LaO/TiO_2, differing only in the relative positions of the oxygen vacancy and the heterointerface. The curves in the right panel of each subplot represent the localized ionic displacement distribution after complete relaxation of the corresponding superlattice model. Specifically, we take the downward direction as the positive direction of polarization. In general, the localized

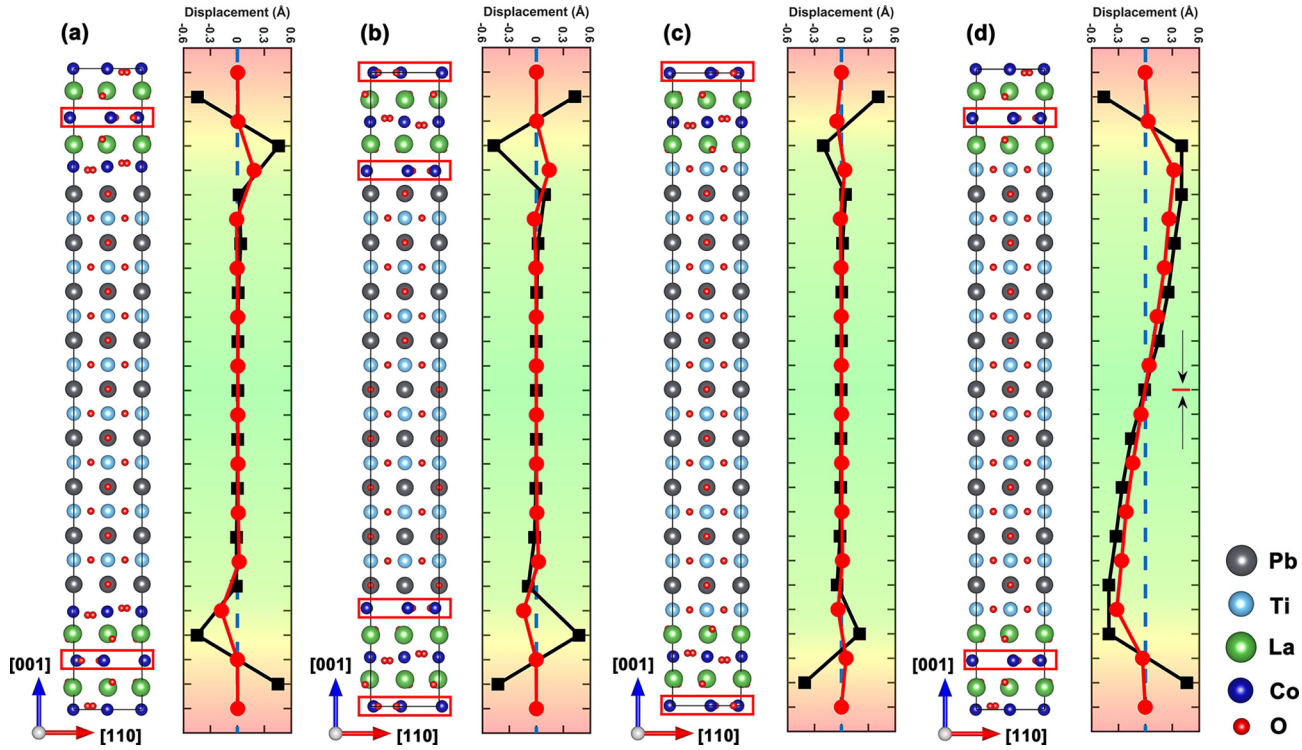

FIG. 2. The schematic diagrams of four prototypes $PbTiO_3/LaCoO_{2.5}$ superlattice models with symmetric interfaces and the ionic displacement profiles of corresponding models after full relaxation. The interface compositions of both (a) and (b) are CoO_x/PbO. The difference is that the positions of oxygen vacancies are in the next-nearest neighbor (a) or at the interface (b). The interface compositions of (c) and (d) are both LaO/TiO_2, the difference being whether the oxygen vacancy layer is close to the heterointerface. The positions of the oxygen vacancy layers are marked with red boxes. In the ionic displacement profiles, the positive values correspond to the downward ionic displacements and the red circles and the black blocks represent the ionic displacements of the BO_x (B = Co or Ti) and the AO (A = La or Pb) layers, respectively.

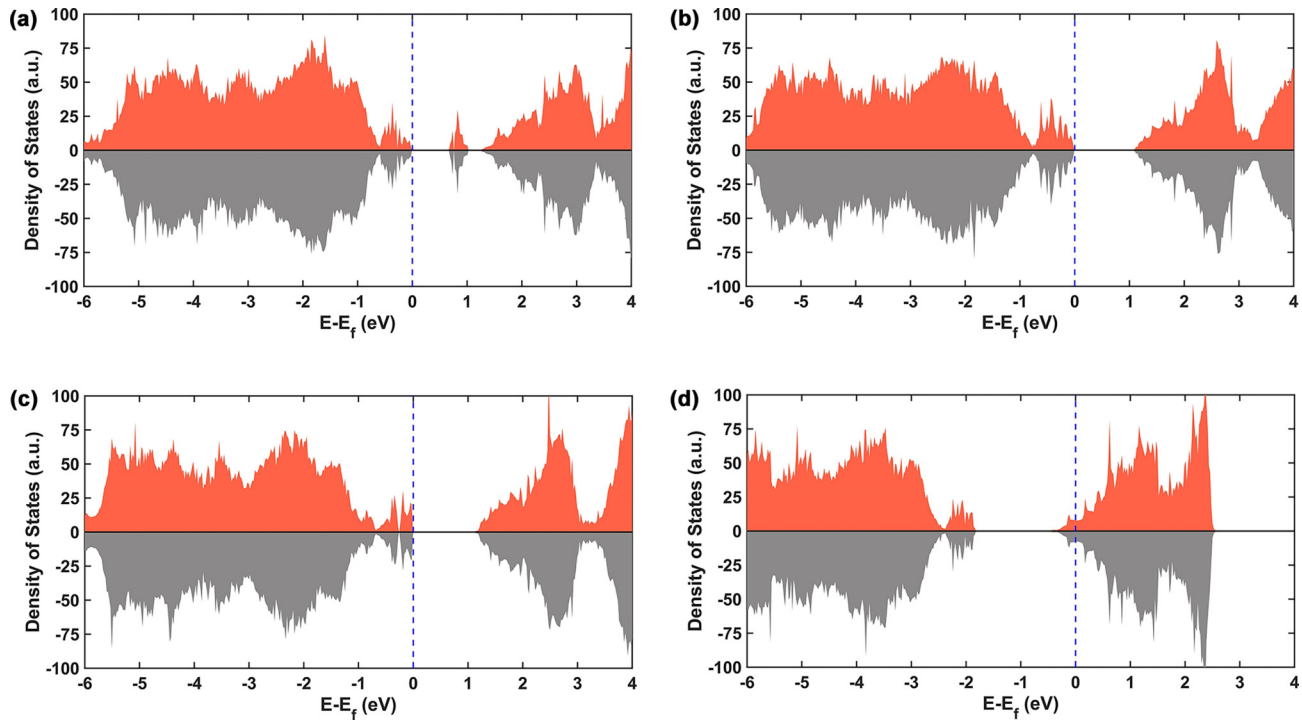

FIG. 3. Density of states corresponding to the superlattice models in Fig. 2. The density of states shown in (a)–(c) is insulated, and in (d) is metallic conducted.

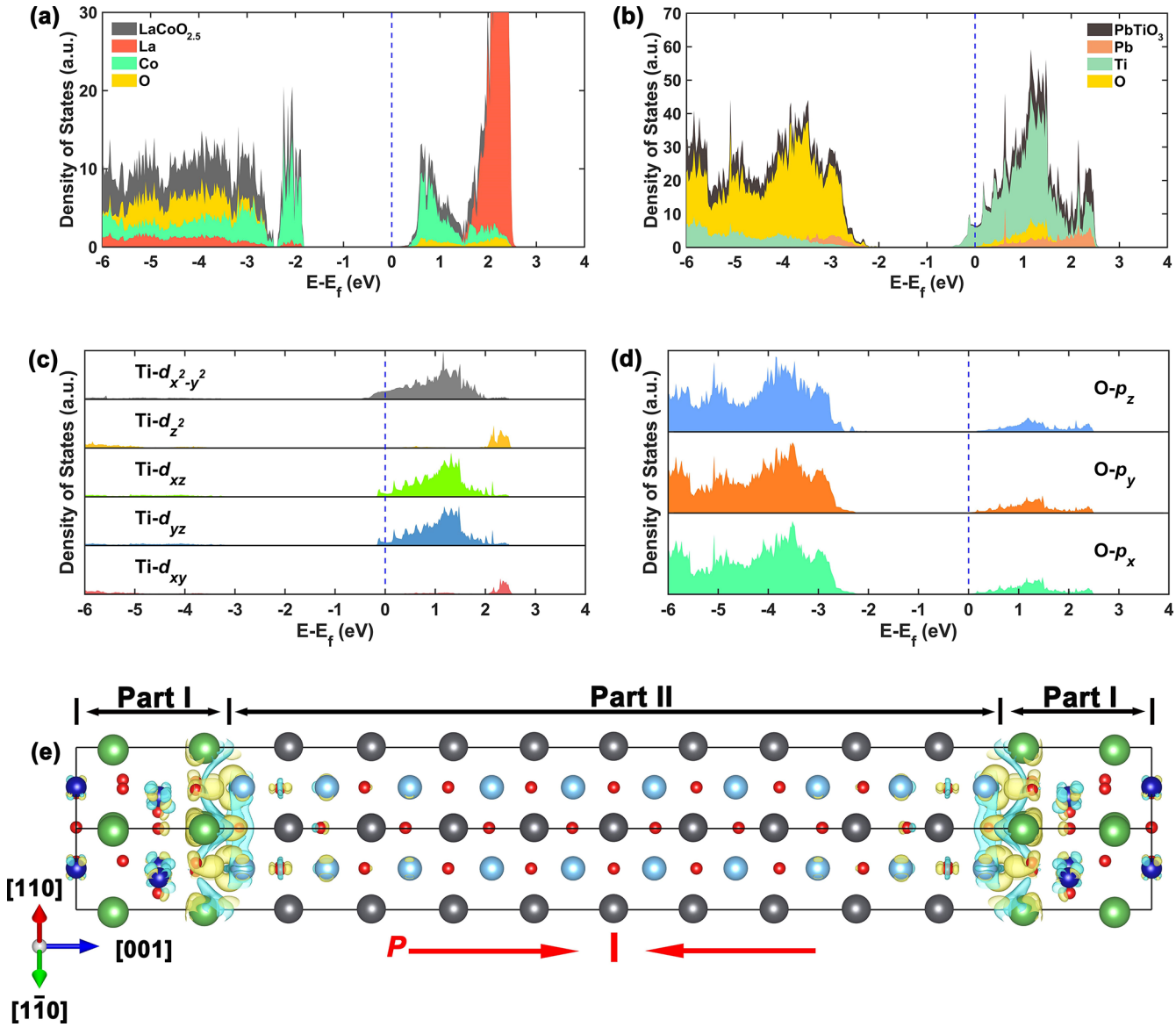

FIG. 4. Electronic structures of the superlattice with the head-to-head CDW. (a) Density of states and contribution of each element in $LaCoO_{2.5}$ layer. (b) Density of states and contribution of each element of $PbTiO_3$ layer. Panels (c) and (d) are various projected densities of states corresponding to the Ti-*d* state and O-*p* state electrons of (b). (e) Schematic diagram of differential charge calculation; yellow for electron gain, and light blue for electron loss. The various parts of differential charge calculations are denoted at the top.

ionic displacement profiles of the four prototypical superlattice models show symmetrical distributions after complete relaxation, which is due to the initial symmetric interface models. As shown in Fig. 2(a), the interfacial CoO_2 layers show obvious ionic displacements, which is caused by the neighboring LaO layers due to the proximity effect. However, all the atomic layers in $PbTiO_3$ possess negligible ionic displacements. The interfacial CoO layer in Fig. 2(b) show small ionic displacements which results in smaller displacements in the neighboring PbO layers and the other atomic layers in $PbTiO_3$ are still in the paraelectric state. The interfacial LaO layers in Fig. 2(c) only show attenuated displacements since these layers are away from the oxygen vacancies and the $PbTiO_3$ layer still maintains the paraelectric state. In contrast, the ionic displacements of the interfacial LaO layers in Fig. 2(d) are still very pronounced due to the neighboring oxygen vacancies. These large ionic displacements successfully induce large polarizations in the $PbTiO_3$ layer. As a result, a head-to-head CDW forms in the $PbTiO_3$ layer.

In addition, we further investigated the electrical properties of the four models, as shown in Fig. 3. The densities of states (DOS) of the models without CDWs all showed insulating behaviors, as shown in Figs. 3(a)–3(c). In contrast, Fig. 3(d) showed a prominent *n*-type conductivity, where the Fermi level passes through the bottom of the conduction band and free electrons act as majority carriers. In addition to the overall evaluation of the conductive properties, we also carried out an in-depth analysis of the electronic structure of the superlattice with CDWs, as shown in Fig. 4. We first calculated the DOS of the $PbTiO_3$ and $LaCoO_{2.5}$ segments in the superlattice and the contribution of various elements to the DOS of different layers. As shown in Fig. 4(a), the Fermi level in the DOS

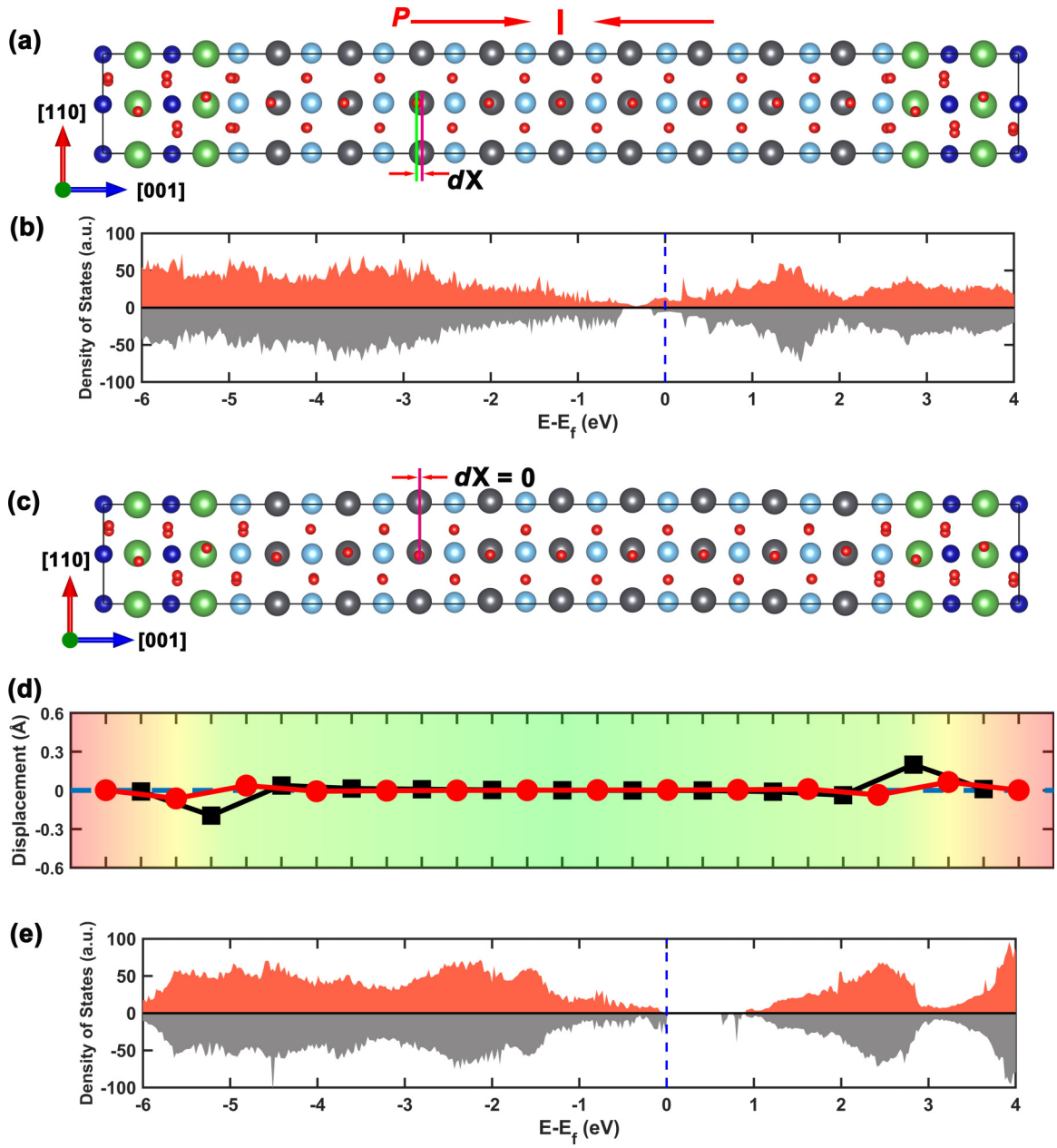

FIG. 5. Schematic diagrams and electrical properties of $PbTiO_3/LaCoO_3$ superlattice model. Panels (a) and (b) are the atomic model and density of states of the initial structure with CDW, respectively. Panel (c) shows the atomic model of the superlattice after fully relaxed. Panel (d) shows the profile of localized ionic displacements of the fully relaxed structure. Panel (e) represents the density of states of the fully relaxed superlattice.

of the $LaCoO_{2.5}$ segment passes through its forbidden band gap, indicating that the $LaCoO_{2.5}$ segment has no contribution to the conductivity of the superlattice. In contrast, as shown in Fig. 4(b), the Fermi level of the $PbTiO_3$ segment passes through the bottom of the conduction band, which suggests that the CDWs in $PbTiO_3$ segment dominates the conductive behavior of the superlattice. In terms of elemental contributions, the distribution of DOS at the Fermi energy level is governed by Ti ions, followed by a tiny distribution of O ions, and Pb ions make no contribution to the conductivity at all. It is worth proposing that only the O ions located in TiO_2 planes contribute to the conductivity, while the O ions in the PbO planes have no contribution to the DOS at the Fermi energy level. Furthermore, we performed a projected DOS analysis on Ti and O ions, as shown in Figs. 4(c) and 4(d). The main contribution to the conductivity is the *d* electrons of Ti, which is in line with q2DEGs in other systems [37,56]. The projected densities of states of Ti-d_{xz} and Ti-d_{yz}, O-p_x and O-p_y in Figs. 4(c) and 4(d) are almost completely identical. To examine the transport mechanism of electrons in the superlattice, we performed differential charge calculations using the method of subtracting the charge densities of the individual parts that make up the system from the charge density of the system, as shown in Fig. 4(e). Differential charge calculation shows that complex and intense electron exchange phenomenon take place at the heterostructure

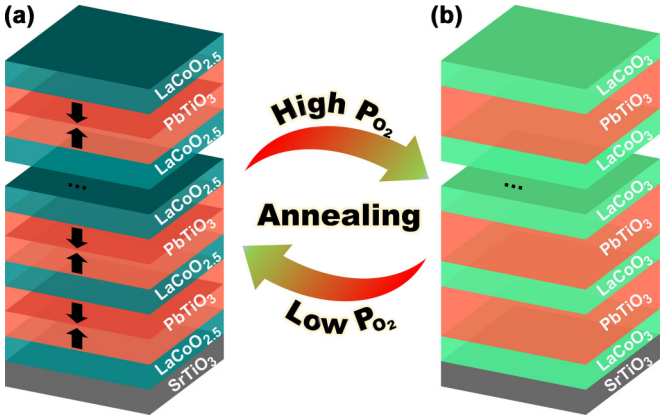

FIG. 6. Schematic diagram of reversible transformation of superlattice under different oxygen partial pressure environments. (a) The $PbTiO_3/LaCoO_{2.5}$ superlattice with CDWs is formed by annealing in a low oxygen partial pressure environment. The black arrows in the $PbTiO_3$ block represent the polarization direction. (b) Annealing in an environment with a high oxygen partial pressure of eliminates the oxygen vacancies and erases the CDWs, forming a $PbTiO_3/LaCoO_3$ superlattice.

interfaces. Further Bader charge analysis of the system shows that about 0.67 e/u.c. are transported from the $LaCoO_{2.5}$ segment to the $PbTiO_3$ segment in the superlattice system. Those electrons transported across the interface play a role in $PbTiO_3$ by screening the positive bound charges in CDW and stabilizing local polarization.

Experimentally, the oxygen vacancies in the lanthanum cobalt oxide system can be eliminated by annealing in an environment of high oxygen pressure [57]. Therefore, we designed a $PbTiO_3/LaCoO_3$ superlattice structure with a preset CDW to investigate the behavior of the CDW after the oxygen vacancies are eliminated, as shown in Fig. 5. Figures 5(a) and 5(b) depict the atomic model and DOS of the initial superlattice with a CDW. Comparing Figs. 5(b) and 3(d), it is found that replacing $LaCoO_{2.5}$ with $LaCoO_3$ mainly affects the valance band and reduces the band gap greatly. The initially preset CDW of the $PbTiO_3$ segment has been erased after complete relaxation and the $PbTiO_3$ segment becomes paraelectric, as shown in the schematic structural diagram in Fig. 5(c) and the localized ionic displacement profile in Fig. 5(d). The result of the density of state calculations indicates that the superlattice system has been transformed into an insulating state, as shown in Fig. 5(e). In other words, after the oxygen vacancies are eliminated, the CDW is erased, accompanied by the metal-insulator transition of the system. It should be emphasized that, as opposed to the previous symmetric distribution of the DOS for spin up and spin down, the DOS here suggests that the overall net magnetic moment of the system is not 0, which is owing to the fact that the stoichiometric $LaCoO_3$ in the tensile strain state is ferromagnetic [46].

Based on the results of theoretical calculations, we propose a technical scheme to the experimental realization of the writing and erasing of the CDW, accompanied by the metal-insulator transition. The superlattice system with symmetric interfaces is constructed as shown in Fig. 6. The CDWs can be written when the superlattice is annealed in a low oxygen partial pressure or vacuum environment, where the system becomes metallic, as shown in Fig. 6(a). When the superlattice system is annealed in high oxygen pressure or pure oxygen environment, the CDWs can be erased, and the system becomes insulating as shown in Fig. 6(b). Indeed, the reversible transformation of $LaCoO_3$ and $LaCoO_{2.5}$ under different oxygen pressures and annealing conditions has been experimentally achieved in the lanthanum cobaltate system [57]. Meanwhile, with the continuing advancement of film growth techniques, precise control of the interface structure in the superlattice or heterojunction system to grow multilayer film systems with symmetric interfaces has also been experimentally achieved [3]. In addition, theoretical calculations reveal that oxygen vacancies in the $PbTiO_3/LaCoO_{2.5}$ heterostructure are more prone to emerge close to the heterogeneous interface [43], which can pin the ionic displacement of the interfacial LaO layers. The major advances in experiments and theoretical calculations mentioned above make the experimental scheme we propose based on the computational results highly feasible.

IV. CONCLUSIONS

In summary, taking advantage of the features that the oxygen vacancy ordering in $LaCoO_{2.5}$ and the symmetric heterogeneous interface can effectively prevent the built-in electric field in the ferroelectric layer, several $LaCoO_{2.5}/PbTiO_3$ superlattice models are constructed, and the head-to-head CDWs form in the $PbTiO_3$ layers in one superlattice model. The CDWs feature typical n-type conductivity characteristics and the electronic structure analysis shows that free electrons accumulate in the vicinity of the CDW to form q2DEG, which screens the positive bound charge of the CDW. The electron transport mechanism involves some of the electrons in the $LaCoO_{2.5}$ transferring across the interface to the $PbTiO_3$ layers. The Ti-d electrons in the proximity of CDWs play a decisive role in the conductivity of the system. Once the vacancies have been eliminated, the CDWs in the superlattice system are erased and the system is transferred to an insulating state. Furthermore, we propose a technical scheme to experimentally realize CDW writing and erasing accompanied with metal-insulator transition from our theoretical calculation results. Our work plays an instrumental role in promoting the development of device based on DWs.

ACKNOWLEDGMENTS

This work was supported by the National Natural Science Foundation of China (Grants No. 52122101 and No. 51971223) and Shenyang National Laboratory for Materials Science (Grants No. L2019R06, No. L2019R08, No. L2019F01, and No. L2019F13). Y.J.W. and Y.L.T. acknowledge the Youth Innovation Promotion Association CAS (Grants No. 2021187 and No. Y202048). Y.L.T. acknowledges the Scientific Instrument Developing Project of CAS (Project No. YJKYYQ20200066).

[1] D. Meier and S. M. Selbach, Ferroelectric domain walls for nanotechnology, Nat. Rev. Mater. **7**, 157 (2022).

[2] P. S. Bednyakov, B. I. Sturman, T. Sluka, A. K. Tagantsev, and P. V. Yudin, Physics and applications of charged domain walls, Npj Comput. Mater. **4**, 65 (2018).

[3] Z. Liu, H. Wang, M. Li, L. Tao, T. R. Paudel, H. Yu, Y. Wang, S. Hong, M. Zhang, Z. Ren *et al.*, In-plane charged domain walls with memristive behaviour in a ferroelectric film, Nature (London) **613**, 656 (2023).

[4] S. Liu, I. Grinberg, and A. M. Rappe, Intrinsic ferroelectric switching from first principles, Nature (London) **534**, 360 (2016).

[5] T. Rojac, H. Ursic, A. Bencan, B. Malic, and D. Damjanovic, Mobile domain walls as a bridge between nanoscale conductivity and macroscopic electromechanical response, Adv. Funct. Mater. **25**, 2099 (2015).

[6] T. Sluka, A. K. Tagantsev, D. Damjanovic, M. Gureev, and N. Setter, Enhanced electromechanical response of ferroelectrics due to charged domain walls, Nat. Commun. **3**, 748 (2012).

[7] J. Seidel, P. Maksymovych, Y. Batra, A. Katan, S. Y. Yang, Q. He, A. P. Baddorf, S. V. Kalinin, C. H. Yang, J. C. Yang *et al.*, Domain wall conductivity in La-doped $BiFeO_3$, Phys. Rev. Lett. **105**, 197603 (2010).

[8] T. Rojac, A. Bencan, G. Drazic, N. Sakamoto, H. Ursic, B. Jancar, G. Tavcar, M. Makarovic, J. Walker, B. Malic *et al.*, Domain-wall conduction in ferroelectric $BiFeO_3$ controlled by accumulation of charged defects, Nat. Mater. **16**, 322 (2017).

[9] C. Godau, T. Kampfe, A. Thiessen, L. M. Eng, and A. Haussmann, Enhancing the domain wall conductivity in lithium niobate single crystals, ACS Nano **11**, 4816 (2017).

[10] S. Y. Yang, J. Seidel, S. J. Byrnes, P. Shafer, C. H. Yang, M. D. Rossell, P. Yu, Y. H. Chu, J. F. Scott, J. W. Ager III *et al.*, Above-bandgap voltages from ferroelectric photovoltaic devices, Nat. Nanotechnol. **5**, 143 (2010).

[11] J. Seidel, L. W. Martin, Q. He, Q. Zhan, Y. H. Chu, A. Rother, M. E. Hawkridge, P. Maksymovych, P. Yu, M. Gajek *et al.*, Conduction at domain walls in oxide multiferroics, Nat. Mater. **8**, 229 (2009).

[12] L. Li, J. Britson, J. R. Jokisaari, Y. Zhang, C. Adamo, A. Melville, D. G. Schlom, L. Q. Chen, and X. Pan, Giant resistive switching via control of ferroelectric charged domain walls, Adv. Mater. **28**, 6574 (2016).

[13] R. G. P. McQuaid, M. P. Campbell, R. W. Whatmore, A. Kumar, and J. M. Gregg, Injection and controlled motion of conducting domain walls in improper ferroelectric Cu-Cl boracite, Nat. Commun. **8**, 15105 (2017).

[14] Q. Huang, J. Yang, Z. Chen, Y. Chen, M. J. Cabral, H. Luo, F. Li, S. Zhang, Y. Li, Z. Xie *et al.*, Formation of head/tail-to-body charged domain walls by mechanical stress, ACS Appl. Mater. Interfaces **15**, 2313 (2022).

[15] J. Jiang, Z. L. Bai, Z. H. Chen, L. He, D. W. Zhang, Q. H. Zhang, J. A. Shi, M. H. Park, J. F. Scott, C. S. Hwang *et al.*, Temporary formation of highly conducting domain walls for non-destructive read-out of ferroelectric domain-wall resistance switching memories, Nat. Mater. **17**, 49 (2018).

[16] H. Y. Sun, J. R. Wang, Y. S. Wang, C. Q. Guo, J. H. Gu, W. Mao, J. F. Yang, Y. W. Liu, T. T. Zhang, T. Y. Gao *et al.*, Nonvolatile ferroelectric domain wall memory integrated on silicon, Nat. Commun. **13**, 4332 (2022).

[17] P. Sharma, D. Sando, Q. Zhang, X. X. Cheng, S. Prosandeev, R. Bulanadi, S. Prokhorenko, L. Bellaiche, L. Q. Chen, V. Nagarajan *et al.*, Conformational domain wall switch, Adv. Funct. Mater. **29**, 1807523 (2019).

[18] J. R. Whyte and J. M. Gregg, A diode for ferroelectric domain-wall motion, Nat. Commun. **6**, 7361 (2015).

[19] S. Pöykkö and D. J. Chadi, *Ab initio* study of 180° domain wall energy and structure in $PbTiO_3$, Appl. Phys. Lett. **75**, 2830 (1999).

[20] B. Meyer and D. Vanderbilt, *Ab initio* study of ferroelectric domain walls in $PbTiO_3$, Phys. Rev. B **65**, 104111 (2002).

[21] Y. H. Shin, I. Grinberg, I. W. Chen, and A. M. Rappe, Nucleation and growth mechanism of ferroelectric domain-wall motion, Nature (London) **449**, 881 (2007).

[22] J. C. Wojdeł and J. Íñiguez, Ferroelectric transitions at ferroelectric domain walls found from first principles, Phys. Rev. Lett. **112**, 247603 (2014).

[23] Y. J. Wang, D. Chen, Y. L. Tang, Y. L. Zhu, and X. L. Ma, Origin of the Bloch-type polarization components at the 180° domain walls in ferroelectric $PbTiO_3$, J. Appl. Phys. **116**, 224105 (2014).

[24] Y. J. Wang, J. Y. Li, Y. L. Zhu, and X. L. Ma, Phase-field modeling and electronic structural analysis of flexoelectric effect at 180° domain walls in ferroelectric $PbTiO_3$, J. Appl. Phys. **122**, 224101 (2017).

[25] X. Y. Zhang, B. Wang, Y. Z. Ji, F. Xue, Y. Wang, L. Q. Chen, and C. W. Nan, First-principles calculations of domain wall energies of prototypical ferroelectric perovskites, Acta Mater. **242**, 118351 (2023).

[26] T. Sluka, A. K. Tagantsev, P. Bednyakov, and N. Setter, Free-electron gas at charged domain walls in insulating $BaTiO_3$, Nat. Commun. **4**, 1808 (2013).

[27] J. J. Gong, C. F. Li, Y. Zhang, Y. Q. Li, S. H. Zheng, K. L. Yang, R. S. Huang, L. Lin, Z. B. Yan, and J. M. Liu, Interactions of charged domain walls and oxygen vacancies in $BaTiO_3$: A first-principles study, Mater. Today Phys. **6**, 9 (2018).

[28] M. P. Campbell, J. P. V. McConville, R. G. P. McQuaid, D. Prabhakaran, A. Kumar, and J. M. Gregg, Hall effect in charged conducting ferroelectric domain walls, Nat. Commun. **7**, 13764 (2016).

[29] M. J. Han, Y. L. Tang, Y. J. Wang, Y. L. Zhu, J. Y. Ma, W. R. Geng, Y. P. Feng, M. J. Zou, N. B. Zhang, and X. L. Ma, Charged domain wall modulation of resistive switching with large ON/OFF ratios in high density $BiFeO_3$ nano-islands, Acta Mater. **187**, 12 (2020).

[30] W.-Y. Wang, Y.-L. Tang, Y.-L. Zhu, Y.-B. Xu, Y. Liu, Y.-J. Wang, S. Jagadeesh, and X.-L. Ma, Atomic level 1D structural modulations at the negatively charged domain walls in $BiFeO_3$ films, Adv. Mater. Interfaces **2**, 1500024 (2015).

[31] I. Stolichnov, L. Feigl, L. J. McGilly, T. Sluka, X. K. Wei, E. Colla, A. Crassous, K. Shapovalov, P. Yudin, A. K. Tagantsev *et al.*, Bent ferroelectric domain walls as reconfigurable metallic-like channels, Nano Lett. **15**, 8049 (2015).

[32] M. Y. Gureev, A. K. Tagantsev, and N. Setter, Head-to-head and tail-to-tail 180° domain walls in an isolated ferroelectric, Phys. Rev. B **83**, 184104 (2011).

[33] J. Sifuna, P. Garcia-Fernandez, G. S. Manyali, G. Amolo, and J. Junquera, First-principles study of two-dimensional electron and hole gases at the head-to-head and tail-to-tail 180° domain

walls in $PbTiO_3$ ferroelectric thin films, Phys. Rev. B **101**, 174114 (2020).

[34] Z. Fu, H. Chen, Y. Liu, M. Liu, and W.-M. Liu, Interface-induced ferroelectric domains and charged domain walls in $BiFeO_3/SrTiO_3$ superlattices, Phys. Rev. B **103**, 195301 (2021).

[35] E. A. Eliseev, A. N. Morozovska, G. S. Svechnikov, V. Gopalan, and V. Y. Shur, Static conductivity of charged domain walls in uniaxial ferroelectric semiconductors, Phys. Rev. B **83**, 235313 (2011).

[36] Y. N. Zuo, Y. A. Genenko, and B. X. Xu, Charge compensation of head-to-head and tail-to-tail domain walls in barium titanate and its influence on conductivity, J. Appl. Phys. **116**, 044109 (2014).

[37] G. Sanchez-Santolino, J. Tornos, D. Hernandez-Martin, J. I. Beltran, C. Munuera, M. Cabero, A. Perez-Munoz, J. Ricote, F. Mompean, M. Garcia-Hernandez *et al.*, Resonant electron tunnelling assisted by charged domain walls in multiferroic tunnel junctions, Nat. Nanotechnol. **12**, 655 (2017).

[38] P. S. Bednyakov, T. Sluka, A. K. Tagantsev, D. Damjanovic, and N. Setter, Formation of charged ferroelectric domain walls with controlled periodicity, Sci. Rep. **5**, 15819 (2015).

[39] U. Petralanda, M. Kruse, H. Simons, and T. Olsen, Oxygen vacancies nucleate charged domain walls in ferroelectrics, Phys. Rev. Lett. **127**, 117601 (2021).

[40] C. H. Park and D. J. Chadi, Microscopic study of oxygen-vacancy defects in ferroelectric perovskites, Phys. Rev. B **57**, 13961(R) (1998).

[41] W. R. Geng, X. H. Tian, Y. X. Jiang, Y. L. Zhu, Y. L. Tang, Y. J. Wang, M. J. Zou, Y. P. Feng, B. Wu, W. T. Hu *et al.*, Unveiling the pinning behavior of charged domain walls in $BiFeO_3$ thin films via vacancy defects, Acta Mater. **186**, 68 (2020).

[42] X. H. Tian, Y. J. Wang, Y. L. Tang, Y. L. Zhu, and X. L. Ma, The effect of oxygen vacancy plate on the domain structure in $BiFeO_3$ thin films by phase field simulations, J. Appl. Phys. **127**, 094102 (2020).

[43] N. B. Zhang, Z. Fang, Y. L. Zhu, Y. J. Wang, Y. L. Tang, M. J. Zou, and X. L. Ma, Interface engineering of oxygen vacancy ordering in an oxide superlattice, J. Phys. Chem. C **126**, 20627 (2022).

[44] N. Zhang, Y. Zhu, D. Li, D. Pan, Y. Tang, M. Han, J. Ma, B. Wu, Z. Zhang, and X. Ma, Oxygen vacancy ordering modulation of magnetic anisotropy in strained $LaCoO_{3-x}$ thin films, ACS Appl. Mater. Interfaces **10**, 38230 (2018).

[45] N. Zhang, X. Tian, Y. Zhu, Y. Wang, Y. Tang, M. Zou, J. Ma, Y. Feng,W. Geng, Y. Cao *et al.*, Thickness dependence of oxygen vacancy ordering in strained $LaCoO_{3-x}$ thin films, J. Phys. Chem. C **124**, 12492 (2020).

[46] D. C. Meng, H. L. Guo, Z. Z. Cui, C. Ma, J. Zhao, J. B. Lu, H. Xu, Z. C. Wang, X. Hu, Z. P. Fu *et al.*, Strain-induced high-temperature perovskite ferromagnetic insulator, Proc. Natl. Acad. Sci. USA **115**, 2873 (2018).

[47] N. Biškup, J. Salafranca, V. Mehta, M. P. Oxley, Y. Suzuki, S. J. Pennycook, S. T. Pantelides, and M. Varela, Insulating ferromagnetic $LaCoO_{3-\delta}$ films: A phase induced by ordering of oxygen vacancies, Phys. Rev. Lett. **112**, 087202 (2014).

[48] W. L. Huang, Q. S. Zhu, W. Ge, and H. Z. Li, Oxygen-vacancy formation in $LaMO_3$ (M = Ti, V, Cr, Mn, Fe, Co, Ni) calculated at both GGA and GGA plus U levels, Comput. Mater. Sci. **50**, 1800 (2011).

[49] A. M. Ritzmann, M. Pavone, A. B. Munoz-Garcia, J. A. Keith, and E. A. Carter, *Ab initio* DFT plus U analysis of oxygen transport in $LaCoO_3$: The effect of Co^{3+} magnetic states, J. Mater. Chem. A **2**, 8060 (2014).

[50] Y. L. Lee, J. Kleis, J. Rossmeisl, and D. Morgan, *Ab initio* energetics of $LaBO_3$(001) (B = Mn, Fe, Co, and Ni) for solid oxide fuel cell cathodes, Phys. Rev. B **80**, 224101 (2009).

[51] G. Kresse and J. Furthmuller, Efficiency of ab-initio total energy calculations for metals and semiconductors using a plane-wave basis set, Comput. Mater. Sci. **6**, 15 (1996).

[52] J. Hafner, Materials simulations using VASP—a quantum perspective to materials science, Comput. Phys. Commun. **177**, 6 (2007).

[53] J. P. Perdew, A. Ruzsinszky, G. I. Csonka, O. A. Vydrov, G. E. Scuseria, L. A. Constantin, X. L. Zhou, and K. Burke, Restoring the density-gradient expansion for exchange in solids and surfaces, Phys. Rev. Lett. **100**, 136406 (2008).

[54] O. H. Hansteen, H. Fjellvag, and B. C. Hauback, Crystal structure and magnetic properties of $La_2Co_2O_5$, J. Solid State Chem. **141**, 411 (1998).

[55] O. H. Hansteen, H. Fjellvag, and B. C. Hauback, Crystal structure, thermal and magnetic properties of $La_3Co_3O_8$ phase relations for $LaCoO_{3-\delta}$ at 673 K, J. Mater. Chem. **8**, 2081 (1998).

[56] K. D. Fredrickson and A. A. Demkov, Switchable conductivity at the ferroelectric interface: Nonpolar oxides, Phys. Rev. B **91**, 115126 (2015).

[57] Q. C. An, Z. Xu, Z. Z. Wang, M. Meng, M. X. Guan, S. Meng, X. T. Zhu, H. Z. Guo, F. Yang, and J. D. Guo, Tuning of the oxygen vacancies in $LaCoO_3$ films at the atomic scale, Appl. Phys. Lett. **118**, 081602 (2021).